Received: 14 December 2022 | Accepted: 26 April 2023

DOI: 10.1002/ppj2.20073

The Plant Phenome Journal OPEN ACCESS

SPECIAL SECTION: NORTH AMERICAN PLANT PHENOTYPING NETWORK (NAPPN) PROC. 2022

Three-dimensional phenotyping of peach tree-crown architecture utilizing terrestrial laser scanning

Jordan Knapp-Wilson[1] | **Rafael Bohn Reckziegel**[2] | **Srijana Thapa Magar**[3] | **Alexander Bucksch**[4,5,6,7] | **Dario J. Chavez**[1,3]

[1]Institute of Plant Breeding, Genetics, Genomics (IPBGG), University of Georgia, Griffin, Georgia, USA

[2]Forest Growth and Dendroecology, University of Freiburg, Freiburg, Germany

[3]Department of Horticulture, University of Georgia, Griffin, Georgia, USA

[4]Department of Plant Biology, University of Georgia, Athens, Georgia, USA

[5]Warnell School of Forestry and Natural Resources, University of Georgia, Athens, Georgia, USA

[6]Institute of Bioinformatics, University of Georgia, Athens, Georgia, USA

[7]School of Plant Sciences, University of Arizona, Tucson, AZ, USA

Correspondence
Alexander Bucksch, School of Plant Sciences, University of Arizona, Tucson, AZ 85721, USA.
Email: bucksch@arizona.edu

Dario J. Chavez, Institute of Plant Breeding, Genetics, Genomics (IPBGG), University of Georgia, Griffin, GA 30223, USA.
Email: dchavez@uga.edu

Assigned to Associate Editor David Ertl.

Funding information
NSF CAREER, Grant/Award Number: 1845760; USDOE ARPA-E ROOTS, Grant/Award Number: DE-AR0000821

Abstract

Tree training systems for temperate fruit have been developed throughout history by pomologists to improve light interception, fruit yield, and fruit quality. These training systems direct crown and branch growth to specific configurations. Quantifying crown architecture could aid the selection of trees that require less pruning or that naturally excel in specific growing/training system conditions. Regarding peaches [*Prunus persica* (L.) Batsch], access tools such as branching indices have been developed to characterize tree-crown architecture. However, the required branching data (BD) to develop these indices are difficult to collect. Traditionally, BD have been collected manually, but this process is tedious, time-consuming, and prone to human error. These barriers can be circumnavigated by utilizing terrestrial laser scanning (TLS) to obtain a digital twin of the real tree. TLS generates three-dimensional (3D) point clouds of the tree crown, wherein every point contains 3D coordinates (*x*, *y*, *z*). To facilitate the use of these tools for peach, we selected 16 young peach trees scanned in 2021 and 2022. These 16 trees were then modeled and quantified using the open-source software *TreeQSM*. As a result, "in silico" branching and biometric data for the young peach trees were calculated to demonstrate the capabilities of TLS phenotyping of peach tree-crown architecture. The comparison and analysis of field measurements (in situ) and in silico BD, biometric data, and quantitative structural model branch uncertainty data were utilized to determine the reconstructive model's reliability as a source substitute for field measurements. Mean average deviation when comparing young tree (YT) height was approx. 5.93%, with crown volume was approx. 13.26% across both 2021 and 2022. All point clouds of the YTs in 2022 showed residuals lower than 12 mm to cylinders fitted to all branches, and mean surface coverage greater than 40% for both the trunk and primary branching orders.

1 | INTRODUCTION

Nearly all fruit tree breeding programs focus on traditional complex traits, such as fruit yield, fruit quality, disease resistance, and freezing prevention/chilling requirements. However, tree-crown architectural traits that could be used to optimize physiological processes and tree training are less understood (Carrillo-Mendoza et al., 2010). This point is especially true for deciduous fruit trees, such as peach [*Prunus persica* (L.) Batsch].

Tree-crown architecture (here referred to simply as tree architecture) can be used as a term that encompasses the dynamic changes in morphology and growth exhibited by a tree throughout its life span (Hallé et al., 1978; Tomlinson, 1983). Being a dynamic process, tree architecture is inherently a highly adaptive and plastic trait, influenced greatly by resource availability (e.g., phytonutrients, water, and light). This results in a wide variety of architectural forms occurring in nature and being optimized around diverse environmental pressures (Farnsworth et al., 1995). Advances in molecular genetics and more accessible genome sequencing technologies have led to an increased focus on identifying the genetic origins of these tree-crown architecture variations (Busov et al., 2008; Groover, 2005). However, many of these architectural forms are not conducive to planned agriculture and orchard management, possessing innate architectures that are too vigorous or crown architectures that inhibit production (Lauri et al., 1997). This problem can be addressed by several approaches, either by direct human intervention in the form of coordinated pruning and shaping (tree training systems; Lauri, 2002), or by reducing/controlling the innate architectures common in modern cultivars (dwarfing rootstocks; Pilcher et al., 2008; Reighard et al., 2011).

Tree training systems have been developed to control the innate architecture of trees. Training systems have proven effective and are utilized in nearly all commercial orchard settings. Nevertheless, these systems are not without their limitations. Establishing a successful training system is laborious and requires the trees to undergo regular pruning. Research that prioritizes an improved understanding of tree architecture, leading to a reduction of pruning costs, has become a priority (Carrillo-Mendoza et al., 2010; Rosati et al., 2013). Unfortunately, conducting research into tree architecture has been challenging due to the physical limits regarding collecting branching data (BD; Bucksch, 2014). Advances in TLS technology provide solutions for these limitations and motivate the use of automated three-dimensional (3D) modeling pipelines (Sadeghian et al., 2022).

Algorithms to compute and quantify BD have been constantly improved over the past decade (Bucksch et al., 2010; Paturkar et al., 2021). Recording BD (for our study, the number of branching orders [BOs] in a tree, and the number of branches per BO) via manual methods is prone to human error and is exceedingly time-consuming. Therefore, developing a new way to record BD without the difficulties of manual collection could lead to breakthroughs in fruit tree physiology and breeding. Studies with access to reliable and readily available BD could focus on quantifying specific traits associated with tree architecture (Barthélémy & Caraglio, 2007). The main focus of our study is to evaluate the use of terrestrial laser scanning (TLS; terrestrial LiDAR) to collect BD from peach trees (Shihua et al., 2016; Lau et al., 2018). This data-retrieval approach is then assessed by analyzing ground-truth data against the original point cloud to validate the in silico results. Finally, the in silico results are compared with the in situ field measurements.

Core Ideas

- Tree training systems were quantified with terrestrial laser scanning.
- The use of TreeQSM was introduced to the horticulture community.
- The authors developed a fast way to discover phenotypes of tree-crown architectures.

TLS technology was utilized to generate 3D point cloud data of peach trees. The utilization of 3D TLS data paired with 3D modeling in orchard settings has been receiving increased attention, due to their potential to assist in the parameterization of plants and to reduce the human labor required (Méndez et al., 2016; Nguyen et al., 2016; Nielsen et al., 2012; Escolà et al., 2017). Point clouds can be used in modeling software to characterize specific phenotypic characteristics of tree structure and architecture (Burt et al., 2013; Li et al., 2017).

The *TreeQSM* software has been used to reconstruct tree architecture as quantitative structural models (QSMs) from digitized trees (Åkerblom, 2017; Bohn Reckziegel et al., 2022; Raumonen, 2020). These QSMs provide biometric data and BD (Lau et al., 2018), which are vital for branching indices or any other method used to quantify tree architecture (Carrillo-Mendoza et al., 2010). *TreeQSM* employs the given TLS-derived point clouds of individual trees to generate quantifiable cylinder approximations of the branches forming the tree architecture (Bohn Reckziegel et al., 2021). These quantifications can then be used as traits characterizing the tree architecture phenotype.

The goal of our study was to successfully model the tree branch structure of peach trees with *TreeQSM* and validate it with ground measurements. Parameters in *TreeQSM* are often optimized for each input point cloud (Raumonen, 2020). However, as our young trees (YTs) are grown under the same training system design, parameters were optimized specifically for young peach trees grown in an open-vase

training system. For all new point cloud generated data, tree models require the optimization of QSM-input parameters as each project will have many sources of variation (i.e., tree structure, sampling with TLS, and processing). Therefore, our study demonstrates the impact TLS has as a quick and relatively cost-effective method for employing high-throughput plant phenotyping (HTPP) in horticultural research and breeding. The cost-effectiveness of TLS stems from the reduced need for labor to collect BD. From our experience, one hour of TLS data collection with one person compares to an entire day and several workers recording BD manually. Eventually, we hope to use the results from *TreeQSM* to help supplement future research in genomics, agrobotics, and HTPP (Raumonen, 2020). While evaluating the uses of *TreeQSM* as a potential HTPP tool for peaches, this study also investigates potential differences in tree architecture among peach trees planted on two commercial rootstocks "Guardian" (Gd) and "MP29." These rootstocks have different effects on peach tree vigor, as well as a possible effect on tree architecture (Beckman et al., 2012).

2 | METHODS

2.1 | Field location and plant material

Our experiment was conducted at UGA Griffin Campus, Peach Research and Extension Orchard, located at Dempsey Farm, University of Georgia, Griffin, GA, USA (33°24′85″N, 84°30′06″W). The peach trees in our study are of the cultivar "Julyprince" grafted onto rootstocks MP29 and Gd. These YTs were produced by growing the rootstocks in a greenhouse setting and budding them on June–July 2019. Plants were grown in one-gallon containers until the following spring and then transplanted to the orchard in April 2020. The soil at the Peach Research and Extension Orchard is a Cecil sandy loam. Eighty YTs were planted, with a spacing of 4.5 m between individual trees and 6 m between rows (Magar et al., 2022). These were equally divided between the Gd and MP29 rootstocks (40/rootstock) across five rows containing 16 trees each in a split-plot randomized complete block design (Thapa Magar et al., 2022). The trees were pruned into an open-vase training system after planting, following the recommended guidelines (Smith et al., 2016). The resulting trees primarily consisted of a short trunk with approximately four or five main leaders or "scaffolds" per tree. For our study, 16 YTs (here on referenced as YT; YTs) were selected for scanning in both 2021 and 2022: YTs 17–24, 29–32, and 41–44. Of these 16 trees, YTs 17–20 and 41–44 were grafted on MP29 rootstock, whereas YTs 21–24 and 29–31 were grafted on Gd rootstock. These trees were selected from multiple areas of the designated split-plot field. Selection for which trees to include in this study was based on availability of scans from both the years 2021 and 2022, where in 2021 only various parts of the split-plot field were fully scanned (Supporting Information 1).

2.2 | Biometric and branching data

2.2.1 | In situ data

Biometric field measurements have been collected at multiple time points every year, since the trees were transplanted. These measurements included tree height, crown width (within and across row), and trunk diameter. From the in situ crown width measurements, crown volume (crV) was calculated. Likewise, in situ BD were also collected for the trees in February 2021. Tree height was collected in the field by using a long-pole measuring stick, with a minimum unit of measure of 1 cm. The crV was calculated as described by Thapa Magar et al. (2022), wherein other biometric measurements, such as crown diameter (both in- and across row) and tree height, were employed. Furthermore, the methods for collecting the various other biometric measurements are defined in Thapa Magar et al. (2020).

In situ BD were collected by counting the number of respective BOs per tree, as well the as the number of branches per BO. The determination and counting of BOs were conducted in a fashion consistent with *TreeQSM*, with the first BO of every tree being the trunk. As our trees are trained in an open-vase configuration, each individual scaffold can be considered a primary branch (i.e., first-order branch). Subsequent bifurcations from these primary branches resulted in secondary branches, with the process repeating until no further bifurcations were observed. The number of branches recorded as first-, second-, or another BO were then totaled to provide a measurement of branches per BO. This process of denoting BOs is also utilized by *TreeQSM* and is illustrated in Figure 1.

2.2.2 | In silico data

The YTs were scanned in February 2021 and February 2022, when they were dormant (under leaf-off conditions and before winter pruning). The terrestrial laser scanner FARO Focus3D X 330 (FARO Technologies, Lake Mary, FL, USA) was used to scan the trees from multiple scan locations, with a scan time of 11 min and 29 s being kept constant throughout each sampling campaign. Basic laser settings used when scanning with the FARO Focus3D scanner were a scan size of 10,240 × 4267, color settings enabled, exposure metering = horizon weighted, selected sensors: inclinometer, compass, altimeter, and GPS, and scanner lens height at 142 cm. Six or more spherical targets were used during the scanning campaigns (200 mm diameter spheres), whereas a minimum of three spheres remained in place from one scan to

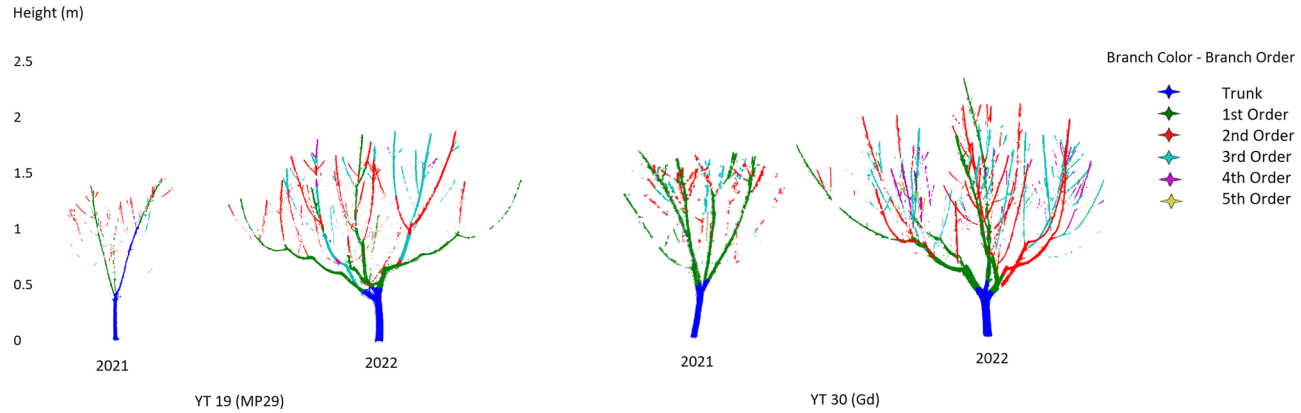

FIGURE 1 Individual tree point clouds of young tree (YT) 19 and YT 30 from 2021 to 2022, respectively. Branches are colorized and denoted by their corresponding branching order. On the far left shows the relative height in meters.

the next to maintain points of reference for scan registrations. The average distance between scan locations was approximately 4.5 m, as the scans were taken between the respective YTs, approximately 3.8 m away from the tree trunk. When moving from one row to the next, the average distance was closer to approx. 6 m, corresponding to the distance between the young-tree rows.

The software FARO SCENE v2022. 1.0 (FARO Technologies, Lake Mary, FL, USA) was used to process the raw scans and conduct the point cloud co-registration. The scans were separated into the respective projects according to year. Processing the scans for both seasons included options to remove stray points, edge and scan artifacts, and a distance filter. These options were selected, with no modifications being made from the parameters suggested in SCENE. The option dark-point processing, which removes points if under a specified lumen reflectance, was excluded due to the overcast weather conditions during both scanning periods. The stray-point filter option checks distances between nearby scan points to establish a uniform 2D grid cell among the processed scans.

Scan registration was first conducted with pre-aligned scans to achieve faster convergence of the automatic registration procedure provided by FARO SCENE. The pre-aligned registration also involved manually verifying the identification of the spherical scan targets between scans. At times of misregistration by SCENE, manual correspondence was used to force identification between two known targets. Following the pre-aligned registration, a second cloud–cloud registration was conducted to minimize distances between estimated center points of the spherical targets. Mean point error for the 2021 registration was 6.7 mm, and in 2022 the mean point error was 11.8 mm. Lastly, point clouds of each YT were manually segmented from the registered point cloud for both project years, using the auto-clipping box tool in SCENE. The data were exported for reconstruction with *TreeQSM* in the xyz format.

2.2.3 | Tree architecture

Similar to other literature sources that have utilized *TreeQSM* for tree architecture reconstruction, the procedure we employed followed three distinct objectives after scan processing and registration (Jin et al., 2022; Lau et al., 2018). These steps were as follows: (a) exporting and cubical down-sampling individual tree point clouds; (b) optimizing the *TreeQSM* input parameters for the 3D reconstruction (for peach trees grown in an open-vase training system); and (c) analyzing the QSMs in silico data and determination of model reliability. The selected trees were exported and processed in CloudCompare (v2.12 alpha, 2020), for nonwoody points, such as ground and extraneous vegetation. A noise-free tree point cloud is necessary for *TreeQSM* to produce accurate models (Raumonen, 2020). Cubical down-sampling is when a voxel grid is used to reduce the density of the 3D point cloud. We down-sampled the individual tree point clouds at a uniform density with cubic voxels of side length 1.7 cm. This was done to ensure the homogenization of the point cloud data, with the side length of 1.7 cm being selected based on previous literature and adjusted for our younger peach trees (Bohn Reckziegel et al., 2022).

2.3 | QSM reconstruction

2.3.1 | TreeQSM input parameters

Although *TreeQSM* has previously been used to model other temperate fruit crops such as apple trees (Zhang et al., 2020), no work has been conducted to the same extent regarding peaches. To remedy this deficiency, *TreeQSM* input parameters first needed to be optimized for the acquired point clouds to provide accurate in silico models, and thus accurate data. The modeling approach has several input parameters to define the cylinder reconstruction of a QSM, with *TreeQSM* v2.4

TABLE 1 Parameters used for young peach trees in 2021 and 2022, respectively.

Year	PatchDiam1 (m)	PatchDiam 2Min (m)	PatchDiam 2Max (m)
2021	0.12	0.02	0.06
2022	0.15	0.02	0.07

(Raumonen, 2020) specifically denoting three input parameters to be optimized: PatchDiam1, PatchDiam2Min, and PatchDiam2Max (Kunz et al., 2017; Raumonen, 2020). PatchDiam1 is responsible for the initial cover-set fitting of the 3D model. This initial fitting defines the trunk and the rough outline of the tree's branching structure. The PatchDiam2 Min and Max parameters are arguably the most important regarding model fitting, as they determine the second cover-fit accuracy and heavily influence primary and higher BO structure. The initial and final cover fittings are constructed around randomly generated voxels that replace the original cloud points for branch segmentation. These three input parameters directly affect the size of these voxels. *TreeQSM* constructs patches of branch surfaces from these voxels as an initial cover set. A second reconstruction process computes cylinders from the cover set to represent in situ branch limbs. In silico biometric data, such as tree height and crV, are then derived from the least-squares fitted cylinders.

Input parameters were optimized for each individual point cloud of the two peach trees, for both years of data collection, following the optimization guidelines of *TreeQSM*'s manual (Raumonen, 2020). Three reasonable values were selected for each key input parameter, and a simple grid search tested the resulting 27 unique combinations of model parameters, with over 20 unique models generated for each combination (a total of 540 models per tree point cloud). The QSM-derived tree parameters were compared to the measurements from the point cloud data. The point-cylinder distance was used as a suitable metric to select the optimal model input parameters. The cylinder distance compares the distance between the fitted cylinders and the original point cloud, whereas the lowest mean cylinder distance value defines the optimal QSM, and the optimal parameters, see Table 1. After optimization, we computed 40 QSM replications per individual tree. This was done as means to overcome randomization elements of the *TreeOSM* algorithms, with the trait measurements of each individual tree then being averaged across the 40 digital replicates. *TreeQSM* is inherently stochastic in its modeling process. Our trials revealed that 40 modeling repetitions yielded an acceptable amount of variation between replicates. Furthermore, these replicates were selected only from models that fit the open-vase training system BO (1 trunk, 3–7 scaffolds).

2.3.2 | Data comparison and validation

As the QSMs are generated, quantitative data are collected following the geometric reconstruction process. Although the scope of in silico data generated after the cylinder fittings is wide ranging, focus was placed on collecting and analyzing biometric data (i.e., tree height and crV) and BD. For the 16 YTs in this study, 40 digital replicates with optimal parameters were executed for each tree for both years. The respective averages and standard deviations were calculated from the 40 replications for the tree height, crV, and BD. Outliers were discarded before initial calculations, that is, models that did not fit the open-vase training system BO, until the 40 replications reflected the open-vase model reconstruction.

After estimating the tree parameters with QSMs (in silico measurements), the in situ data collected were used as reference when comparing the data (ground truth). The mean absolute deviation (MAD) percentage scores were calculated to describe the error of estimation between the in silico and in situ data. This process was conducted for the biometric data for MP29 YTs 18 and 19 and Gd YTs 30 and 31 for both years, as well for the BD from all trees in 2021. Utilizing MAD scores to validate computational models has been reported previously. The MAD score is defined as Jin et al. (2022) as follows:

$$MAD = \left| \frac{Q - R}{R} \right| \times 100\%,$$

where Q is the mean of the in silico generated biometric data BD, and R is the collected in situ ground truth data.

2.3.3 | Examining uncertainty in QSM reconstruction

TreeQSM includes metrics to quantify the quality of the QSMs by comparing biometric statistics between the computed cylinder models and the tree point clouds. Two of these metrics are point–cylinder distance, which is used to determine the optimal parameters for model generation, and the average surface coverage (%) of the cylindrical model (regarding the origin point cloud). Both metrics were calculated following the model creation and included results for the tree architecture segments: trunk, branch, 1branch, and 2branch. These segments correspond to measurements from the tree trunk, all BOs of the tree (excluding the trunk), first-order branches, and second-order branches. The mean values for both cylinder distance and average surface coverage were calculated from the 40 individual tree models and were analyzed as another metric to reveal model reliability (Knapp-Wilson et al., 2021).

2.4 | Analysis of rootstock effects on architecture

Utilizing BD generated from QSMs of all YTs 2022 point cloud data, a preliminary analysis was conducted to investigate potential effects different rootstocks may impart on the branch morphology of the trees. This investigation included the analysis of the avg. number of branches per tree, branches per BO, and BOs per tree, all as a function of their respective rootstocks. BD collection was gathered and averaged among the 40 replicates per YT. The BD were collected from the generated QSMs, which utilized the optimized parameters listed earlier. A one-way analysis of variance (ANOVA) was also done to determine the statistical significance of the findings from this preliminary analysis.

3 | RESULTS

3.1 | Initial 3D model reconstructions

In situ BD proved much easier to collect from younger trees in 2021 than in 2022. The less-intricate tree architecture of the 2021 trees enabled us to measure the entire architecture and branching structure accurately by hand. Therefore, in situ BD were only collected during 2021. This point is evident in the tree models generated from the 2022 point clouds, as they possessed more complex tree architecture overall. This difference in crown complexity is especially noticeable when considering that the YTs have been in the field for only 1 year between scanning campaigns (Figure 1). This resulted in numerous model replications to achieve the correct designation of BOs. However, after 1 year in the field the complexities in their tree architecture increased and noticeable differences between rootstocks were visually apparent. Drastic changes in tree architecture should be expected from vigorous scion/rootstock combinations, such as Julyprince/Gd (as seen in YT 30). However, more branches in the crown resulted in a slower convergence of digital replications constructed via the *TreeQSM* modeling process. We also observed that a higher surface density of the point cloud results in fewer modeling errors. When surface density was lower, a wider range of extreme outliers were recorded, such as with the scans taken during 2021.

3.2 | Analysis and comparison of in situ and in silico data

3.2.1 | Biometric data

The in silico data (average 40 model replications) of YTs 18, 19, 30, and 31 from 2021 and 2022 were calculated. The differences in the MAD scores between the in situ and in silico data were noted for tree height and crV. The differences were minimal, with the largest MAD difference percentage score (est. of error) being for YT 18 and YT 31 regarding crV in 2021, being 25.15% and 31.56% for the years 2021, respectively; see Table 2. The reasons for the observed variation are differences between the time points when size measurements were taken and the first pruning of the YTs. For 2021, the average crV MAD percentages were the highest out of both categories for both years (18.97%).

Another source of this difference could be attributed to the 2021 scans not correctly recording all the thin, still-growing branches during field measurements. Typically, objects smaller than 0.5 cm in diameter are difficult for TLS scanners to detect accurately (Hackenberg et al., 2015). The YTs during this period were still juvenile; perhaps, smaller branches could have been included in field measurements, affecting crown width. This under-sampling of branches could explain the decrease in MAD scores from 2021 to 2022 for all YTs across both crV and tree height.

3.2.2 | Branching data

The models generated from our YT scans during 2021 were used to gather in silico BD and compared with in situ BD from the field. The MAD scores were generated for all BOs for four of the YTs in our study (2 MP29, 2 Gd; Table 3). These MAD scores essentially compare the number of recorded branches found in the field with the number generated from *TreeQSM* across the 40 model replications. The MAD scores for four of the YT models shown in Table 3 had a MAD of >1 branch at the first BO, and a MAD of >4 branches at the second BO. At subsequently higher BOs (third and fourth), the MAD scores comparing the in situ BD and the in silico BD were also found to be >4 branches (except for YT 19 at the third BO). However, the MAD percentages were much greater at higher BOs. The average MAD percentages were found to climb as BOs increased. The MAD percentage difference between the second and third BOs was approx. 15%. However, even with the MAD percentage error above 50% at higher BOs, this does not translate into large differences in the expected number of branches. Examining the MAD scores, which list the expected variability of branches from the reference (in situ) field data, the differences at these higher BOs do not exceed an average of 2.41 branches at the third BO and 2.03 branches at the fourth BO.

The MAD values and scores are partitioned across the four main BOs for four selected YTs in 2021. The MAD scores here specifically refer to the number of branches, with the MAD percentages corresponding to the percentage difference

TABLE 2 Comparisons of tree height and crown volume of reconstructed peach trees.

Metric	Variable	Unit	YT18 (MP29) 2021	YT18 (MP29) 2022	YT19 (MP29) 2021	YT19 (MP29) 2022
Tree height	Mean (in silico)	m	0.99	1.80	1.74	1.84
	Reference (in situ)	m	1.04	1.82	1.83	1.8
	MAD	m	0.06	0.03	0.10	0.05
	MAD score	%	5.43	1.67	5.25	2.71
crV	Mean	m^3	0.16	2.14	0.65	2.67
	Reference	m^3	0.21	2.35	0.71	2.86
	MAD	m^3	0.05	0.22	0.07	0.21
	MAD score	%	25.15	9.38	10.36	7.17
Metric	**Variable**	**Unit**	**YT30 (Gd) 2021**	**YT30 (Gd) 2022**	**YT31 (Gd) 2021**	**YT31 (Gd) 2022**
Tree height	Mean (in silico)	M	1.77	2.52	1.71	2.47
	Reference (in situ)	M	1.91	2.25	1.80	2.70
	MAD	M	0.14	0.27	0.09	0.23
	MAD score	%	7.11	11.91	5.01	8.37
crV	Mean	m^3	0.79	6.47	0.76	5.33
	Reference	m^3	0.86	6.67	1.11	5.91
	MAD	m^3	0.08	0.26	0.35	0.58
	MAD score	%	8.81	3.84	31.56	9.78

Abbreviations: crV, crown volume; Gd, guardian; MAD, mean absolute deviation.

TABLE 3 Branching data comparison for four trees measured in 2021.

Metric	Tree	Unit	First BO	Second BO	Third BO	Fourth BO
MAD branch	YT19	Branch no.	0.20	3.60	5.20	2.55
	YT20	Branch no.	0.55	2.15	1.75	1.10
	YT29	Branch no.	0.40	3.05	1.15	3.30
	YT30	Branch no.	0.20	1.90	1.55	1.15
	AVG	Branch	0.34	2.68	2.41	2.03
MAD score	YT19	%	5.00	18.95	52.00	51.00
	YT20	%	13.75	10.24	25.00	27.50
	YT29	%	8.00	9.84	7.19	55.00
	YT30	%	5.00	7.92	22.14	23.00
	AVG	%	7.94	11.74	26.58	39.13

Abbreviations: BO, branching order; MAD, mean absolute deviation.

between the reference data (in situ) and the computational data (in silico).

Reviewing 2021 data in Table 2 reveals a difference between the YT19 (grown on an MP29 rootstock) and YT30 (grown on Gd rootstock) rates of growth. The differences regarding the number of branches between in situ and in silico sources lie within a standard deviation of the reference data, that being the in situ values. These are seen from both the MP29 and Gd rootstocks (Figure 2). In 2022, however, the differences between the two rootstocks grew substantially. Gd rootstocks are known to be a high-vigor rootstock, with an approximate difference of 110 branches between in silico Gd and MP29 in the cumulative BD from 2022, shown later in Figure .

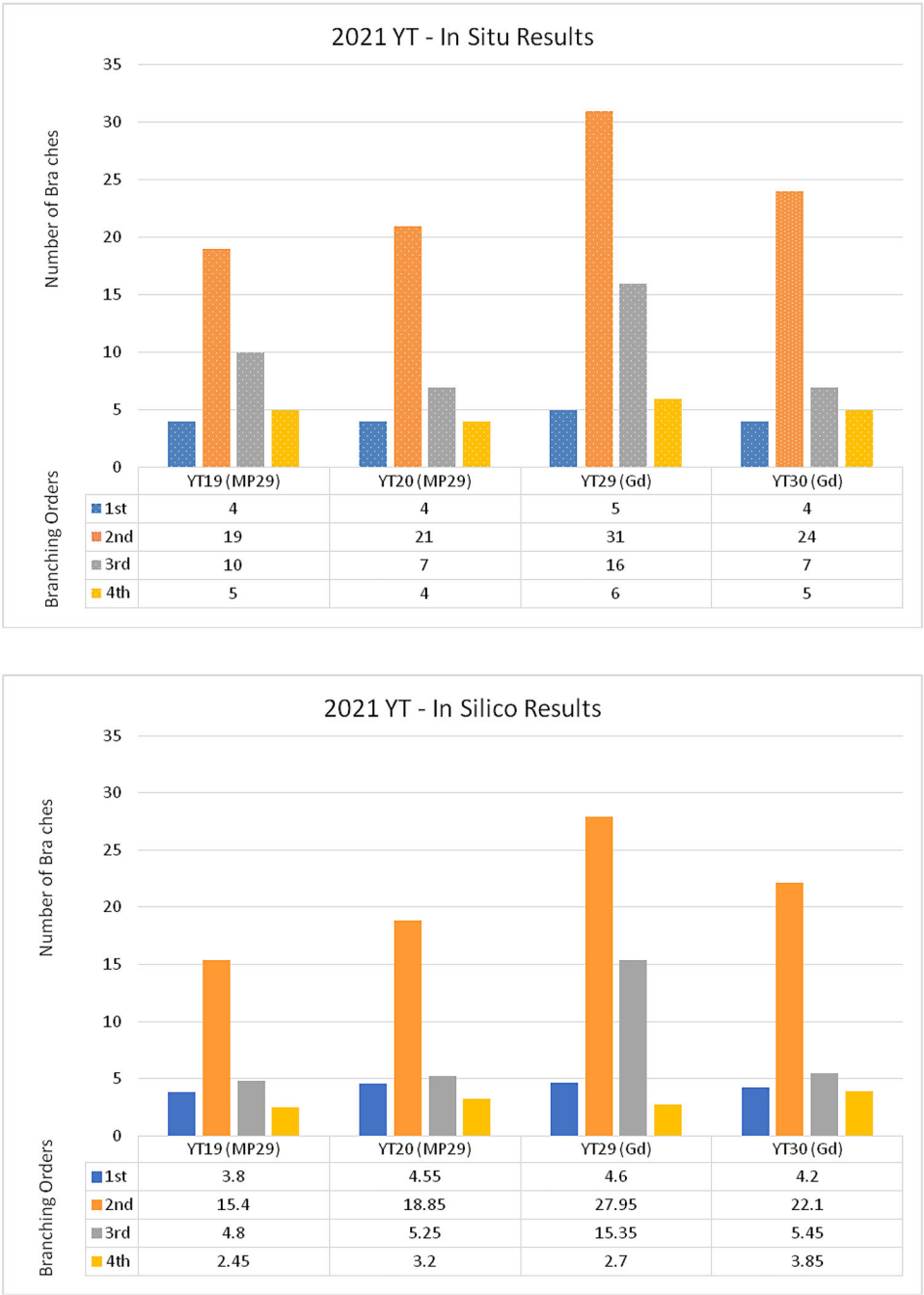

FIGURE 2 Comparison of in silico (bottom, solid color) and in situ (top, patterned) branching data from young trees (YTs) 19, 20, 29, and 30. Trees 19 and 20 are Julyprince varieties grafted on the MP29 rootstock, whereas trees 29 and 30 are also Julyprince but grafted onto guardian (Gd) rootstock.

3.3 | Analysis of the in situ branching data and residual metrics

After successfully generating models for all the YTs and optimizing the QSM parameters, the results from the QSM reconstruction of the specified YTs include biometric data, BD, and QSM branch uncertainty metrics, which as referenced previously, are cylinder distance (mm) and cylinder surface coverage (%). These two metrics were compiled from the 40 digital replications in *TreeQSM* for the YT 2021 scans. The values from these metrics are displayed in Figure 3. The categories that *TreeQSM* delineates the residual data into are based on the BOs for each tree: trunk, all branch, first branch, and second branch. These metrics have been used previously to derive modeling and data accuracy from QSM cylinder recreation (Knapp-Wilson et al., 2021). The difference in

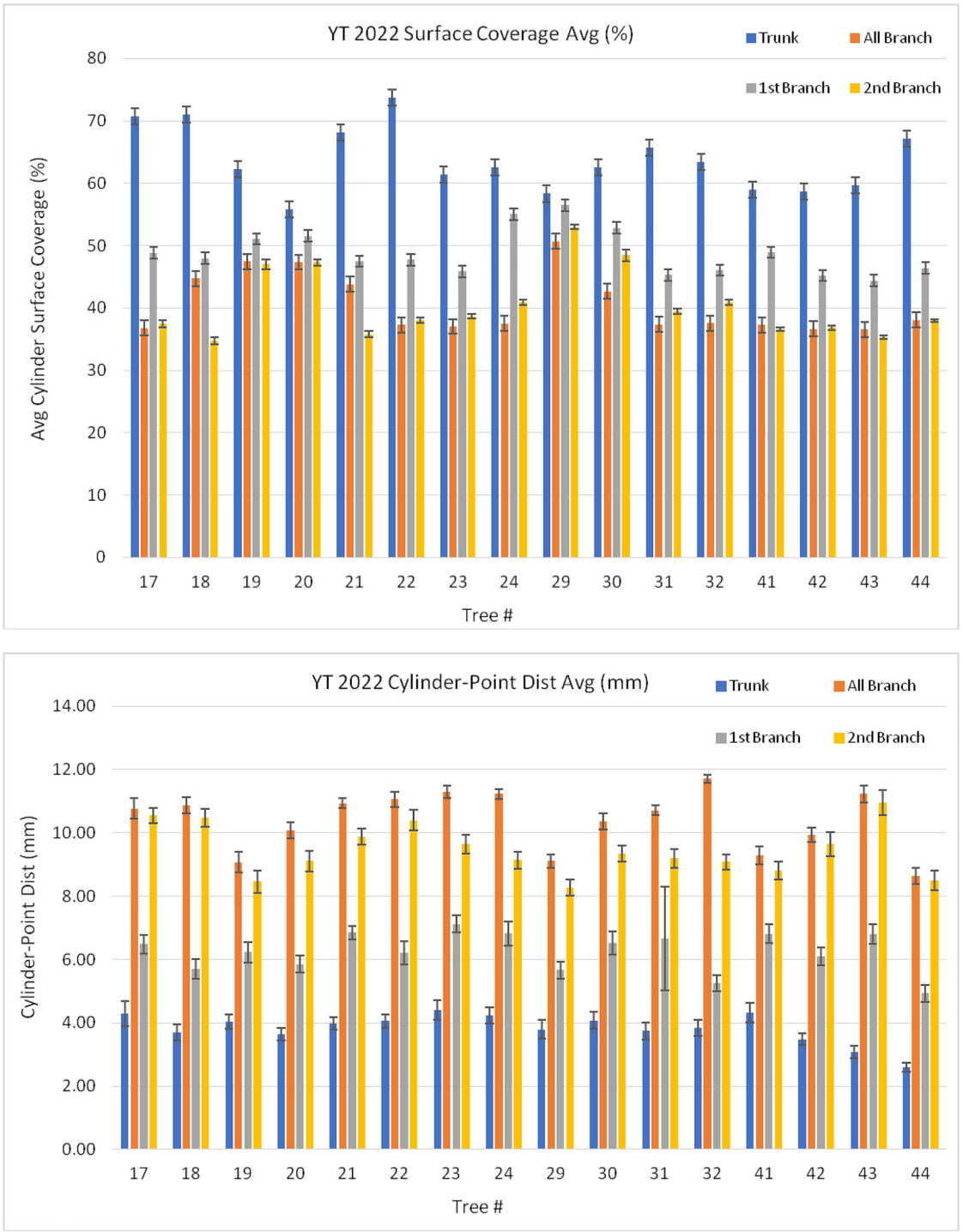

FIGURE 3 *TreeQSM* input optimization metrics from the 2022 young trees (YTs), represented as the cylinder distance (avg. distance between the original point cloud data and the resulting quantitative structural model (QSM) cylindrical reconstruction, top), and the surface coverage average (bottom). All the averages were computed from 40 digital replications for each tree, with standard error visualized with error bars. These metrics can also be used as measurements of QSM uncertainty during branch reconstruction.

vigor between the two rootstocks is already perceivable at this early stage of development.

This is illustrated in Figure 3, which shows that all the trees from 2022 (YT 17–24, 29–32, 41–44) had cylinder surface coverages for both trunk and first-order branches above 40%, and the more complicated second-order branches had a surface coverage above 35%. The YTs with Gd rootstocks (21–24, 29–32) showed better results when compared with MP29 rootstocks (17–20, 41–44) in terms of cylinder coverage fitting. The Gd rootstock trees showed that the

highest point cylinder surface area averages for all metrics, with the higher cylinder coverage metrics, might be related to the more vigorous branching nature that Gd rootstocks possess. Increased vigor, which leads to more robust architecture, results in a greater surface density in the point cloud data of Gd trees when scanned. The larger point density then results in an informed small-cover-set generation during initial reconstruction in *TreeQSM*. Although the more informed small-cover generation might result in greater cylinder coverage percentages, the denser cloud point density can also lead to a higher distance between the point cloud and the 3D cylinder segmentations created during the geometric reconstruction process (Figure 3).

In addition to cylinder coverage, the cylinder distance measurements of the reconstructed cylindrical models were below 12 mm for all metrics, with trees only having their "All Branch" and "2nd Branch" categories going above 10 mm. Overall, the mean surface coverage average % for all BOs, from all trees in 2022, was found to be slightly over 40% (40.56%). All trees also had their trunk surface coverage >60% (63.76%), with the mean "first branch" metric almost hitting 50% among all 2022 tree scans (48.83%). Both of these QSM branch uncertainty metric values are consistent with previous findings for TLS reconstructive models, especially in peach trees (Hackenberg et al., 2015; Knapp-Wilson et al., 2021).4

3.4 | Subsequent BD and emerging trends

In silico BD were collected in addition to QSM branch uncertainty metrics, with the results from all the YTs scanned during 2022 illustrated later. The BD presented in Figure 4 were obtained from QSMs that were generated from the beforementioned optimized input parameters. Analysis of the BD reveals noticeable architectural differences emerging between the Gd and MP29 rootstocks. Differences in branch number and branching morphology can be seen clearly in Figure 4. In the 2021 point cloud data, the YTs were under 2 years old, still in the early stages of tree growth. In 2022, the differences in total branches, vigor, and tree architecture—quantified by the difference in second- and third-order branch numbers between the two trees—have increased. Producing in silico 3D models of peach trees that reveal differences of even one to five branches at higher BOs might still be useful for supplying larger, aggregate BD that can be used in genomic studies regarding tree architecture. Another note of interest is the different rates at which the YTs develop, depending on which rootstock they were grafted upon (Figure 1).

The trees with the Gd rootstock not only experienced considerable increases across all BOs but also possessed the most branches within the third BO: approx. 25 more branches than the next largest BO. In contrast, trees grafted on the MP29 rootstocks had relatively minimal growth between 2021 and 2022. The growth that occurred was mainly around the third BO, with an approx. average of 15 more branches than in 2021. The MP29 trees also experienced more growth in higher BOs, producing fifth and sixth BOs, when none were recorded in 2021. The major difference between the two rootstocks is that the largest number of branches in the MP29 trees still appeared within the second BO, which contrasts with the Gd trees where the largest number of branches were found in the third BO. Whether this phenomenon is a result of slow third BO growth, an effect of the training system, or a trend that will remain consistent remains to be tested and will need to include a larger pool of samples.

TABLE 4 Analysis of variance (ANOVA) of branch number per branching order (BO) as a function of rootstock for all 2022 young trees (YTs).

Independent variable	Response variable	*F* statistic	*p* value
Rootstock (Gd, MP29)	First BO	0.287	0.599
	Second BO	21.87	2.53e − 4
	Third BO	75.44	1.88e − 7
	Fourth BO	46.33	4.21e − 6
	Fifth BO	24.03	1.59e − 4
	Sixth BO	13.88	0.00184
	Total branch no.	51.28	2.26e − 6

Abbreviation: Gd, guardian.

A statistical ANOVA was done in order to test the significance of the effect the respective rootstocks, Gd or MP29, had on the number of branches shown in Figure 4. This was broken down as analysis done for the total number of branches per tree, as well as number of branches per BO. Like in Figure 4, all YT 2022 BD were used for this analysis, in addition to the mean values collected for all Gd and MP29 trees, respectively. The results of the variance analysis are seen in Table 4. The first BO in this analysis can be seen as a control, wherein all trees have the same 4–5 scaffolds as per the open-vase training system. The same bound where used during modeling as well, with model replicates being accepted if having a first BO number between 3 and 6. As such, the first BO reported a *p*-value of 0.599, above the traditionally accepted alpha of 0.05. The subsequent BOs however all reported *p*-values far less than 0.05, with the smallest value being recorded for the third and fourth BOs, respectively.

4 | DISCUSSION AND CONCLUSIONS

In our study, we evaluated the accuracy of in silico data to quantify branching geometry in peach trees using TLS. The QSM-derived tree parameters were compared with previously

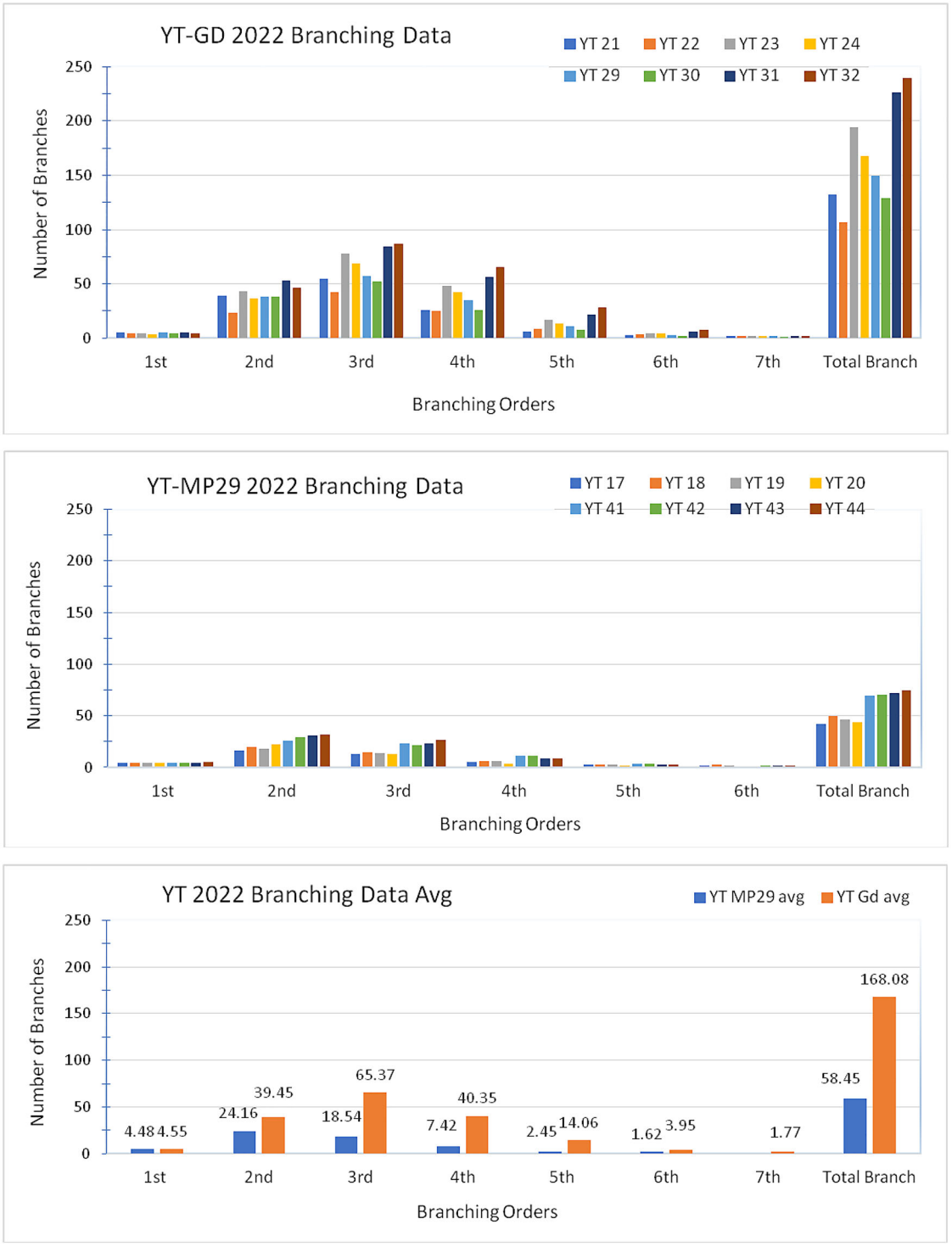

FIGURE 4 Three different histograms graphs representing the averages for all trees in this study, being grouped by guardian (Gd) (top) rootstock, MP29 (bottom) rootstock, and the averages for both Gd and MP29 compared against each other. The differences in the number of branches between the branching orders (BOs) and the structure of BOs can be visibly identified here.

collected in situ data from the field. Altogether, the findings from this study encourage future investigation and study of quantitative modeling approaches regarding peach and its potential agronomic uses. The presented QSM branch uncertainty metrics (cylinder distance and cylinder coverage) are consistent with previous findings and followed results as outlined in the *TreeQSM* manual (Raumonen, 2017). The MAD scores (Tables 1 and 2) varied between the biometric data and the BD but were overall consistent with previous literature that has reported similar margins of error (Jin et al., 2022). The

results from our comparisons of in situ, in silico, and QSM branch uncertainty metrics suggest that *TreeQSM* can produce useful quantitative models for peach trees in an orchard setting. These QSMs can be utilized as an automated replacement for field data measurements and future research into tree architecture.

Our study also showcased the attributes of TLS, which, combined with quantitative modeling, may be of future agronomic use in horticulture. The methodology we employed in this study represents an effective, time-efficient, and comparatively less-laborious approach to phenotyping orchard trees. As our approach removes the human error and labor barrier of manually collecting BD, it is now possible to standardize the collection and recording of such data. In addition, the removal of extraneous human labor means this approach rapidly decreases the time constraints and efficiency of collecting BD. Using TLS as a quick HTPP tool is also economically scalable and easy to learn. A more involved and thorough procedural manual could be released to help facilitate familiarity with the tools and systems. From our experience, BD are most effectively collected during winter months, when the trees have no leaves. During the off-leaf period, one person can efficiently operate TLS scanners to collect dense, point cloud data of the crown architecture. In the future, an online platform could be established, which allows for automated processing and registration of point cloud data. The construction of such an interface would enable growers and researchers to quickly receive quantitative data from their raw point clouds. Examples of such online platforms already exist for root phenotyping (Bonelli et al., 2022), and notable researchers in the tree modeling community have likewise begun calling for the establishment of similar online resources (Hackenberg et al., 2022). Such an online platform could reduce the time and physical resources needed to collect BD, improve the reproducibility of measurements, and create an open-access interface which would open the possibilities of 3D modeling to far more researchers.

Furthermore, research into the areas of tree architecture will become increasingly important, as the need for automation grows, as well as orchard management styles that can accommodate such changes (e.g., high-density orchards, fruiting wall configurations; Medeiros et al., 2017; Nielsen et al., 2012; Wu et al., 2019; Mu et al., 2018). Therefore, the selection of new scion cultivars possessing traits more amenable to these high-density orchard systems will be in greater demand (Hill & Hollender, 2019). The tools demonstrated in our study can be utilized to begin collecting the necessary data.

Similarly, future trends for our research will focus more on the potentially notable difference in branching structure between Gd and MP29 rootstocks. Quantified by the difference in branch numbers and new growth in BOs between the 2021 and 2022 scans, Gd and MP29 rootstocks may have a stronger effect on tree architecture than previously known. At the juvenile stage of development, both the Gd and MP29 rootstocks displayed similar trends in biometric data and BD. When examining tree architecture on the branch level, the majority of branches for the Gd and MP29 trees were found in the second BO. The subsequent BOs with the highest number of branches followed a descending order, with the third and fourth BOs having comparatively fewer branches. This decreasing trend noticeably shifted, however, as evident in the 2022 in situ BD in Figure 4. This shift highlights a potential architectural difference that was largely, if not solely, influenced by the two rootstocks examined in this study. Although it is known that the MP29 rootstock can strongly affect tree vigor, there is no literature available on how these dwarfing rootstocks affect tree architecture (Beckman et al., 2012). In species such as pear and apple, field trials and genomic studies have been conducted to investigate this very question (Friend et al., 2020; Petersen & Krost, 2013; Seleznyova et al., 2008). Many aspects concerning the nature of rootstock/scion interaction and their effects and each other's subsequent architectures (i.e., root and crown architecture) have yet to be investigated. Even less research has been conducted regarding peach trees (Migicovsky et al., 2019; Williams et al., 2021). Therefore, this study might act as a starting point for further field trials, computational modeling, and genomic studies into this area of research for peach. Our data show that the effect of dwarfing rootstocks significantly ($p < 0.00184$ at largest value) reduces the number of branches at all higher level BOs (>first BO) when compared to higher vigor rootstocks. This was shown in Figure 4 and Table 4, where the statistical analysis of the data was also shown to support these findings.

To summarize, our QSMs were found to have a MAD score of approx. 5.93% in regards to tree height, and a MAD score of approx. 13.26% when comparing the in situ and in silico crV data from both 2021 and 2022. For just biometric data from 2022, MAD scores of approximately 6.17% and 7.54% were recorded for tree height and crV, respectively. The observed difference between 2021 and 2022 scores could be the result of the first pruning during 2021 and/or the technical limits of the TLS scanner resolution that causes under-sampling on the fine branches of the YTs. In 2022, the YT point cloud data showed the cylinder distance was <12 mm at nearly BOs, as well as a mean surface coverage >40% across all BOs. Although younger tree scans are more difficult to accurately characterize at higher BOs, first and second BOs were shown to have MAD <8% and <12%, respectively, in 2021 scans. In addition, our 2022 BD showed that dwarfing rootstocks not only result in reduced number of branches per tree but also result in a reduced number of branches at all higher level BOs. Nonetheless, this BD are vital; event at higher BOs, in the process of utilizing TLS technology and QSMs to phenotype peach tree architecture in an automated and reliable manner.

As such, the presented work burgeons the possibility to discover and functionally characterize previously unknown tree architecture phenotypes.

AUTHOR CONTRIBUTIONS

Jordan Knapp-Wilson: Conceptualization; data curation; formal analysis; investigation; methodology; software; validation; visualization; writing—original draft; writing—review and editing. **Rafael Bohn Reckziegel**: Formal analysis; methodology; software; writing—review and editing. **Srijana Thapa Magar**: Investigation; writing—review and editing. **Alexander Bucksch**: Conceptualization; investigation; methodology; software; supervision; writing—original draft; writing—review and editing. **Dario J. Chavez**: Conceptualization; funding acquisition; project administration; supervision; writing—original draft; writing—review and editing.

ACKNOWLEDGMENTS

The research was supported by the NSF CAREER Award No. 1845760 and USDOE ARPA-E ROOTS Award No. DE-AR0000821 to A.B. as well as the Hatch Grant Initiative, UGA Cultivar Development Grants to D.J.C., and John Ingle Award to J.K.W. Any opinions, findings, and conclusions or recommendations expressed in this material are those of the author(s) and do not necessarily reflect those of the funders. The work was in part performed during the transition period of A.B. from the University of Georgia to the University of Arizona.

CONFLICT OF INTEREST STATEMENT

The authors declare no conflicts of interest.

ORCID

Jordan Knapp-Wilson https://orcid.org/0000-0002-3526-3682
Rafael Bohn Reckziegel https://orcid.org/0000-0001-8781-1970
Srijana Thapa Magar https://orcid.org/0000-0003-3599-1767
Alexander Bucksch https://orcid.org/0000-0002-1071-5355
Dario J. Chavez https://orcid.org/0000-0002-1493-2680

REFERENCES

Åkerblom, M. (2017). *Inversetampere/TreeQSM: Initial release*. Zenodo. (https://doi.org/10.5281/zenodo 844626)

Barthélémy, D., & Caraglio, Y. (2007). Plant architecture: A dynamic, multilevel and comprehensive approach to plant form, structure and ontogeny. *Annals of Botany*, *99*(3), 375–407. https://doi.org/10.1093/aob/mcl260

Beckman, T. G., Chaparro, J. X., & Sherman, W. B. (2012). MP29, a Clonal Interspecific Hybrid Rootstock for Peach.

Bohn Reckziegel, R., Larysch, E., Sheppard, J. P., Kahle, H.-P., & Morhart, C. (2021). Modelling and comparing shading effects of 3D tree structures with virtual leaves. *Remote Sensing*, *13*(3), 532. https://doi.org/10.3390/rs13030532

Bohn Reckziegel, R., Mbongo, W., Kunneke, A., Morhart, C., Sheppard, J. P., Chirwa, P., du Toit, B., & Kahle, H. P. (2022). Exploring the branch wood supply potential of an agroforestry system with strategically designed harvesting interventions based on terrestrial LiDAR data. *Forests*, *13*(5), 650. https://doi.org/10.3390/f13050650

Bonelli, W., Liu, S., Cotter, C., Flory, M., Luck, M., & Bucksch, A. (2022). PlantIT: Containerized phenotyping in the cloud. *Authorea*. https://doi.org/10.1002/essoar.10508354.1

Bucksch, A. (2014). A practical introduction to skeletons for the plant sciences. *Applications in plant sciences*, *2*(8), 1400005. https://doi.org/10.3732/apps.1400005

Bucksch, A., & Fleck, S. (2011). Automated detection of branch dimensions in woody skeletons of fruit tree canopies. *Photogrammetric Engineering & Remote Sensing*, *77*(3), 229–240.

Bucksch, A., Lindenbergh, R., & Menenti, M. (2010). SkelTre. *The Visual Computer*, *26*(10), 1283–1300. https://doi.org/10.1007/s00371-010-0520-4

Burt, A., Disney, M. I., Raumonen, P., Armston, J., Calders, K., & Lewis, P. (2013). Rapid characterisation of forest structure from TLS and 3D modelling. In 2013 IEEE International Geoscience and Remote Sensing Symposium-IGARSS (pp. 3387–3390). IEEE.

Busov, V. B., Brunner, A. M., & Strauss, S. H. (2008). Genes for control of plant stature and form. *The New Phytologist*, *177*(3), 589–607.

Carrillo-Mendoza, O., Sherman, W. B., & Chaparro, J. X. (2010). Development of a Branching Index for Evaluation of Peach Seedlings Using Interspecific Hybrids. Retrieved from https://agris.fao.org/agris-search/search.do?recordID=US201301863320

Carrillo-Mendoza, O., Sherman, W. B., & Chaparro, J. X. (2010). Development of a branching index for evaluation of peach seedlings using interspecific hybrids. *Hortscience*, *45*(6), 852–856. https://doi.org/10.21273/HORTSCI.45.6.852

CloudCompare. (2020). *CloudCompare* (version 2.12 alpha) [GPL software]. http://www.cloudcompare.org/

Escolà, A., Martínez-Casasnovas, J. A., Rufat, J., Arnó, J., Arbonés, A., Sebé, F., Pascual, M., Gregorio, E., & Rosell-Polo, J. R. (2017). Mobile terrestrial laser scanner applications in precision fruticulture/horticulture and tools to extract information from canopy point clouds. *Precision Agriculture*, *18*, 111–132.

Farnsworth, K. D., & Niklas, K. J. (1995). Theories of optimization, form and function in branching architecture in plants. *Functional Ecology*, *9*(3), 355–363. https://doi.org/10.2307/2389997

Friend, A. P., Diack, R. N., van Hooijdonk, B. M., Knäbel, M., Tustin, D. S., & Palmer, J. W. (2020). Scion architecture on dwarfing candidate pear rootstocks. *Acta Horticulturae*, *1281*, 153–162. 10.17660/ActaHortic.2020.1281.22

Groover, A. T. (2005). What genes make a tree a tree? *Trends in Plant Science*, *10*(5), 210–214.

Hackenberg, J., Disney, M., & Bontemps, J. (2022). Gaining insight into the allometric scaling of trees by utilizing 3d reconstructed tree models: A SimpleForest study. *BioRxiv*.

Hackenberg, J., Spiecker, H., Calders, K., Disney, M., & Raumonen, P. (2015). SimpleTree—An efficient open source tool to build tree models from TLS clouds. *Forests*, *6*(11), 4245–4294. https://doi.org/10.3390/f6114245

Hallé, F., Oldeman, R. A., & Tomlinson, P. B. (1978). *Tropical trees and forests: An architectural analysis*. Springer Science & Business Media.

Hill, J. L., & Hollender, C. A. (2019). Branching out: New insights into the genetic regulation of shoot architecture in trees. *Current Opinion in Plant Biology*, *47*, 73–80. https://doi.org/10.1016/j.pbi.2018.09.010

Jin, S., Zhang, W., Shao, J., Wan, P., Cheng, S., Cai, S., Cai, S., & Li, A. (2022). Estimation of larch growth at the stem, crown, and branch levels using ground-based LiDAR point cloud. *Journal of Remote Sensing*, *2022*. https://doi.org/10.34133/2022/9836979

Knapp-Wilson, J., Reckziegel, R. B., Bucksch, A., & Chavez, D. (2021). Imaging and quantitative analysis of peach tree branching index via Treeqsm. *HortScience*, 56(9), S248–S249.

Kunz, M., Hess, C., Raumonen, P., Bienert, A., Hackenberg, J., Maas, H. G., Härdtle, W., Fichtner, A., & Von Oheimb, G. (2017). Comparison of wood volume estimates of young trees from terrestrial laser scan data. *iForest: Biogeosciences and Forestry*, *10*(2), 451–458. https://doi.org/10.3832/ifor2151-010

Lau, A., Bentley, L. P., & Martius, C. (2018). Quantifying branch architecture of tropical trees using terrestrial LiDAR and 3D modelling. *Trees*, *32*, 1219–1231. https://doi.org/10.1007/s00468-018-1704-1

Lau, A., Bentley, L. P., Martius, C., Shenkin, A., Bartholomeus, H., Raumonen, P., Malhi, Y., Jackson, T., & Herold, M. (2018). Quantifying branch architecture of tropical trees using terrestrial LiDAR and 3D modelling. *Trees*, *32*(5), 1219–1231. https://doi.org/10.1007/s00468-018-1704-1

Lauri, P. É. (2002). From tree architecture to tree training—An overview of recent concepts developed in apple in France. *Journal-Korean Society for Horticultural Science*, *43*(6), 782–788.

Lauri, P. É., Térouanne, É., & Lespinasse, J. M. (1997). Relationship between the early development of apple fruiting branches and the regularity of bearing—An approach to the strategies of various cultivars. *Journal of Horticultural Sciences*, *72*, 519–530. https://doi.org/10.1080/14620316.1997.11515539

Li, R., Bu, G., & Wang, P. (2017). An automatic tree skeleton extracting method based on point cloud of terrestrial laser scanner. *International Journal of Optics*, *2017*. https://doi.org/10.1155/2017/5408503

Li, S., Wang, J., Liang, Z., & Su, L. (2016). Tree point clouds registration using an improved ICP algorithm based on kd-tree. In 2016 IEEE International Geoscience and Remote Sensing Symposium (IGARSS) (pp. 4545–4548). IEEE.

Medeiros, H., Kim, D., Sun, J., Seshadri, H., Akbar, S. A., Elfiky, N. M., & Park, J. (2017). Modeling dormant fruit trees for agricultural automation. *Journal of Field Robotics*, *34*(7), 1203–1224. https://doi.org/10.1002/rob.21679

Méndez, V., Rosell-Polo, J. R., Pascual, M., & Escolà, A. (2016). Multitree woody structure reconstruction from mobile terrestrial laser scanner point clouds based on a dual neighbourhood connectivity graph algorithm. *Biosystems Engineering*, *148*, 34–47. https://doi.org/10.1016/j.biosystemseng.2016.04.013

Migicovsky, Z., Harris, Z. N., Klein, L. L., Li, M., McDermaid, A., Chitwood, D. H., Fennell, A., Kovacs, L. G., Kwasniewski, M., Londo, J. P., Ma, Q., & Miller, A. J. (2019). Rootstock effects on scion phenotypes in a 'Chambourcin' experimental vineyard. *Horticulture Research*, *6*. https://doi.org/10/1038/s41438-019-0146-2

Mu, Y., Fujii, Y., Takata, D., Zheng, B., Noshita, K., Honda, K., Ninomiya, S., & Guo, W. (2018). Characterization of peach tree crown by using high-resolution images from an unmanned aerial vehicle. *Horticulture Research*, *5*, 74. https://doi.org/10.1038/s41438-018-0097-z.2011.2166780

Nguyen, T. T., Slaughter, D. C., Maloof, J. N., & Sinha, N. (2016). Plant phenotyping using multi-view stereo vision with structured lights. In *Autonomous air and ground sensing systems for agricultural optimization and phenotyping* (Vol. 9866, pp. 22–30). SPIE.

Nielsen, M., Slaughter, D. C., Gliever, C., & Upadhyaya, S. (2012). Orchard and tree mapping and description using stereo vision and lidar. In International Conference of Agricultural Engineering.

Paturkar, A., Sen Gupta, G., & Bailey, D. (2021). Making use of 3d models for plant physiognomic analysis: A review. *Remote Sensing*, *13*(11), 2232. https://doi.org/10.3390/rs13112232

Petersen, R., & Krost, C. (2013). Tracing a key player in the regulation of plant architecture: The columnar growth habit of apple trees (Malus × domestica). *Planta*, *238*, 1–22. https://doi.org/10.1007/s00425-013-1898-9

Pilcher, R. R., Celton, J. M., Gardiner, S. E., & Tustin, D. S. (2008). Genetic markers linked to the dwarfing trait of apple rootstock 'Malling 9.'. *Journal of the American Society for Horticultural Science*, *133*(1), 100–106. https://doi.org/10.21273/JASHS.133.1.100

Raumonen, P. (2017). TreeQSM: Quantitative structure models of single trees from laser scanner data. *MATLAB-Software TreeQSM User Guide v*, *2*, 27.

Raumonen, P. (2020). InverseTampere/TreeQSM (Version 2.4.0). *Zenodo*. https://doi.org/10.5281/zenodo.3482908

Raumonen, P., Kaasalainen, M., Åkerblom, M., Kaasalainen, S., Kaartinen, H., Vastaranta, M., Holopainen, M., Disney, M., & Lewis, P. (2013). Fast automatic precision tree models from terrestrial laser scanner data. *Remote Sensing*, *5*(2), 491–520. https://doi.org/10.3390/rs5020491

Reighard, G. L., Beckman, T., Belding, R., Black, B., Byers, P., Cline, J., Cowgill, W., Godin, R., Johnson, R. S., Kamas, J., Kaps, M., Larsen, H., Lindstrom, T., Ouellette, D., Pokharel, R., Stein, L., Taylor, K., Walsh, C. S., Ward, D., & Whiting, M. (2011). Six-year performance of 14 prunus rootstocks at 11 sites in the 2001 NC-140 peach trial. *Journal of the American Pomological Society*, *65*(1), 26.

Rosati, A., Paoletti, A., Caporali, S., & Perri, E. (2013). The role of tree architecture in super high density olive orchards. *Scientia Horticulturae*, *161*, 24–29. https://doi.org/10.1016/j.scienta.2013.06.044

Sadeghian, H., Naghavi, H., Maleknia, R., Soosani, J., & Pfeifer, N. (2022). Estimating the attributes of urban trees using terrestrial photogrammetry. *Environmental Monitoring and Assessment*, *194*(9), 625.

Seleznyova, A. N., Stuart Tustin, D., & Thorp, T. G. (2008). Apple dwarfing rootstocks and interstocks affect the type of growth units produced during the annual growth cycle: Precocious transition to flowering affects the composition and vigour of annual shoots. *Annals of Botany*, *101*(5), 679–687. https://doi.org/10.1093/aob/mcn007

Smith, E., Westerfield, B., & Chavez, D. (2016). Home Fruit Orchard Pruning Techniques (Circular 1087). Retrieved from University of Georgia Cooperative Extension website. https://extension.uga.edu/publications/detail.html?number=C1087

Thapa Magar, S., Vellidis, G., Porter, W., Liakos, V., Andreis, J. H., & Chavez, D. J. (2022). Development and evaluation of a SmartIrrigation peach app in a young peach orchard. *Acta Horticulturae*, *1352*, 575–582. https://doi.org/10.17660/ActaHortic.2022.1352.78

Thapa Magar, S. T., Chavez, D. J., & Casamali, B. (2020). Soil, leaf and fruit nutritional status of a young peach orchard under different

irrigation and fertilization practices in Georgia. In *2020 ASHS Annual Conference*. ASHS.

Tomlinson, P. B. (1983). Tree architecture: New approaches help to define the elusive biological property of tree form. *American Scientist*, *71*(2), 141–149.

Williams, B., Ahsan, M. U., & Frank, M. H. (2021). Getting to the root of grafting-induced traits. *Current Opinion in Plant Biology*, *59*, 101988. https://doi.org/10.1016/j.pbi.2020.101988

Wu, G., Zhu, Q., Huang, M., Guo, Y., & Qin, J. (2019). Automatic recognition of juicy peaches on trees based on 3D contour features and colour data. *Biosystems Engineering*, *188*, 1–13. https://doi.org/10.1016/j.biosystemseng.2019.10.002

Zhang, C., Yang, G., Jiang, Y., Xu, B., Li, X., Zhu, Y., Lei, L., Chen, R., Dong, Z., & Yang, H. (2020). Apple tree branch information extraction from terrestrial laser scanning and backpack-LiDAR. *Remote Sensing*, *12*(21), 3592. https://doi.org/10.3390/rs12213592

SUPPORTING INFORMATION

Additional supporting information can be found online in the Supporting Information section at the end of this article.

How to cite this article: Knapp-Wilson, J., Bohn Reckziegel, R., Thapa Magar, S., Bucksch, A., & Chavez, D. J. (2023). Three-dimensional phenotyping of peach tree-crown architecture utilizing terrestrial laser scanning. *The Plant Phenome Journal*, *6,* e20073. https://doi.org/10.1002/ppj2.20073